Geometric-Optical Bidirectional Reflectance Modeling of the Discrete Crown Vegetation Canopy: Effect of Crown Shape and Mutual Shadowing

Xiaowen Li and Alan H. Strahler, *Member, IEEE*

***Abstract*—In the case where a vegetation cover can be regarded as a collection of individual, discrete plant crowns (such as forest, woodland, savanna, or shrubland), the geometric-optical effects of the shadows that the crowns cast on the background and on one another strongly condition the brightness of the vegetation cover as seen from a given viewpoint in the hemisphere. At the "hotspot," when illumination and viewing positions coincide, shadows are hidden behind plant crowns and the scene appears bright. As the viewing position diverges from that of illumination, the shadows behind the crowns are progressively revealed and the scene darkens. Because, in general, the shadows will not be circular, the amount of shadow revealed will be a function of both the zenith and azimuth angles by which the viewing and illumination positions diverge, rather than a simple phase angle between them. This effect creates an assymetric hotspot, in which the shape of the hotspot is related to the shape of the plant crowns in the scene. At large zenith angles, mutual shadowing of crowns becomes an important factor. Illumination shadows will tend to fall on other crowns, rather than the background, and will preferentially shadow the lower portions of adjacent crowns. Further, these shadows will be preferentially obscured since adjacent crowns will also tend to obscure the lower portions of other crowns. This effect produces a "bowl-shaped" BRDF in which the scene brightness increases at the function's edges. Our paper derives formulas describing the hotspot and mutual-shadowing effects and presents examples that show how the shape of the BRDF is dependent on the shape of the crowns, their density, their brightness relative to the background, and the thickness of the layer throughout which the crown centers are distributed.**

Keywords—Hotspot, bidirectional reflectance distribution function, plant canopy, vegetation reflectance, reflectance modeling.

NOMENCLATURE

A	Area of the footprint of the sensor's field of view, or pixel size.
A_c	Area of crown surface within A that is both illuminated and viewed, as projected onto the background.
A_g	Area of background within A that is both illuminated and viewed.
A_t	Area of crown surface within A that is not illuminated but viewed, as projected onto the background.
A_z	Area of background within A that is not illuminated but viewed.
b	Vertical half axis of ellipsoid.
C	Average radiation exitance from sunlit crown surface, as viewed by sensor.
F	Ratio Γ_c/Γ for a single crown.
f	Ratio $K_c/(1-K_g)$ for a pixel.
G	Average radiation exitance from sunlit backgorund surface, as viewed by sensor.
h	Variable for height at which a crown center is located.
h_1	Lower bound of height distribution of crown centers.
h_2	Upper bound of height distribution of crown centers.
i	Direction vector of illumination
K_g	Proportionof A_g in A.
K_c	Proportion of A_c in A.
K_t	Proportion of A_t in A.
M	Mutual shadowing proportion.
M_i	Mutual shadowing proportion in the illumination direction.
M_v	Mutual shadowing proportion in the view direction.
n	Count of crown centers distributed in a pixel.
$n(h)$	Density of crown centers per unit area as a function of height within the canopy.
$O(\theta_i, \theta_v, \phi, h)$	Overlap function of view and illumination shadows on ground.
P_i	Conditional probability that a crown surface element will face the viewer given that it is shaded from view.

Manuscript received June 1, 1991; revised September 26, 1991. This work was supported by the National Aeronautics and Space Administration under Grant NAGW-2082, U. S. National Science Foundation under Grant INT-9014263, and the Chinese National Science Foundation under Grant 4880050.

X. Li is with the Institute of Remote Sensing Application, Chinese Academy of Science, Beijing. He is currently located at the Center for Remote Sensing, Boston University, 725 Commonwealth Avenue, Boston, MA, 02215.

A. Strahler is with the Department of Geography and Center for Remote Sensing, Boston University, at the same address.

IEEE Log Number 9105688.

P_o	Overlap area of $P_i M_i \Gamma_v$ and $P_v M_v \Gamma_v$ in fraction ofΓ_v.
P_v	Conditional probability that a crown surface element will face the sun given that it is shaded from view.
R	Horizontal radius of ellipsoid.
$R(i,v)$	Directional reflectance factor.
s	Direction vector for normal of a facet of crown surface, or as variable representing such facet.
T	Average radiation exitance from shaded crown surface, as viewed by sensor.
v	Directional vector for viewing.
Z	Average radiation exitance from shaded background, as viewed by sensor.
B	A parameter indicating the vertical range of distribution of crown centers.
Γ	Area of background shaded in either view or illumination directions by a single ellipsoid.
Γ_c	Area of view and illumination shadow of a single ellipsoid on the background.
Γ_v	Area of view shadow of a single ellipsoid on the background.
θ	Zenith angle.
θ_i	Zenith angle of illumination direction.
θ_i'	Effective zenith angle of illumination direction, adjusted for spheroidal shape of crown.
θ_v	Zenith angle of view direction.
θ_v'	Effective zenith angle of view direction, adjusted for spheroidal shape of crown.
λ	Density of spheroid centers in a pixel or footprint, i.e., n/A.
ϕ	Relative azimuth of illumination and view directions.

I. Introduction

The interaction between electromagnetic radiation and terrestrial plant canopies is a complex phenomenon and a key element in many applications of remote sensing. In recent years, much effort has been devoted to understanding and modeling the dependence of the bidirectional reflectance distribution function (BRDF) of vegetation-covered earth surfaces as a function of various environmental, structural, and physiological conditions as well as viewing and illumination geometries. Typical approaches have included two-stream, radiative transfer, geometric optics, hybrids of two or more of these, and numerical simulation. Some are applicable to continuous vegetation covers, such as crops, while others are best utilized for discontinuous covers such as forests.

To be realistic, all models have to deal with the interactions that occur within and between individual canopies. These can exist on several levels, including single scattering—shadowing of leaves, crowns, and background by leaves and crowns—and multiple scattering among leaves, crowns, and background. The former effect creates the "hotspot," a peak in directional reflectance in the antisolar direction that is commonly observed in vegetation canopies when the sun and observer are at the same position in the hemisphere. It occurs because the leaves, stems and trunks that comprise the plant cover hide their own shadows under these conditions, and thus the scene appears bright due to maximal single scattering.

A. Background

The earliest practical plant canopy reflectance model is that of Suits [1], [2], which adds direct irradiation and directional exitance to a two-stream Kubleka–Monk [3] model. The hotspot is treated as an empirical function reducing the attenuation of exiting radiation as a function of the phase angle between illumination and view directions. The model further assumes that leaves are Lambertian and either vertical or horizontal. It has been extended by Verhoef [4] to the case of variable leaf-angle distribution (the SAIL model), and by Reyna and Bhadwar [5] to include a specular reflectance component. More recently, Jupp and Strahler [6] have added a proper geometric-optical kernel to the Suits model that is driven by leaf shape, arrangement, and spacing.

In classical radiative transfer models, the medium is typically treated as a horizontally uniform series of plane-parallel layers composed of small absorbing and scattering particles. This type of model is well established for the interaction between radiation and the atmosphere [7], but, in the case of a vegetation canopy, the scattering elements (e.g., leaves) are of finite size and thus a pure radiative transfer approach is not possible. Rather, the shadowing behavior that produces the hotspot through enhanced single scattering must be accommodated for a radiative transfer model to be realistic. Sometimes this is included in an empirical phase function for the canopy as a whole [8]; in other treatments, the phase function of the leaf surface is separated from a phase function that describes the hotspot [9]. The hotspot function can take several forms—sometimes fully empirical, other times driven specifically by the shape, orientation, and/or spacing of leaves. Functions include piecewise-linear, negative exponential, trigonometric, and geometric. Examples may be found in models developed by Gerstl [10], [11], Myneni *et al.* [12], [13], and Marshak [14]. Various approximate solutions have also been derived, such as the two-stream solutions of Nilson [15], [16] and Verstraete [9]. These types of models are best applied to continuous vegetation covers, such as crop canopies or homogeneous grasslands.

B. Geometric-Optical Approach

In the geometric-optical approach, the bidirectional reflectance is modeled as a purely geometric phenomenon that results when scenes of discrete, three-dimensional objects are illuminated and viewed from different positions in the hemisphere. The shapes of the objects, their count densities and patterns of placement are the driving variables, and they condition the mixture of sunlit and shaded objects and background that is observed from a particular viewing direction, given a

direction of illumination. This mixture, in turn, controls the brightness apparent to an observer or a radiometric instrument. The objects themselves may be leaves or individual, discrete plant canopies, or, in hybrid models, leaves within discrete canopies. In previous work, we have emphasized the individual tree canopy as the functional element in modeling, and have applied geometric-optical models of bidirectional reflectance successfully for open and moderately closed stands of conifers treated as "green" cones on a contrasting background [17], [18]. Jupp *et al.* [19] used a similar approach for trees as spheroidal objects, and extended the treatment to two crown layers above a background using Boolean logic of Serra [20]. Recently, Strahler and Jupp [21] have provided a more general Boolean treatment that includes leaves within discrete crown envelopes as a two-stage, nested model.

Although the geometric-optical approach properly models the three-dimensional nature of the scene with due complexity, it greatly simplifies the interaction between elements due to multiple scattering among leaves and individual canopies. The reflectance associated with a given viewpoint is treated as an area-weighted sum of four fixed reflectance components—sunlit leaf or canopy, shaded leaf or canopy, sunlit background, and shaded background—whereas radiative transfer theory shows that all of these components are variable. For example, the reflectance of a sunlit canopy will be a function of canopy depth, which will be lesser near the edges of the crown and greater near the center. Thus, the "signature" of sunlit canopy will not be uniform. The signature of shaded canopy will also be nonuniform, as it is related to the radiation penetrating through the crown, the diffuse skylight distribution, and multiply scattered radiation from the ground and other crowns into the shaded portion. Clearly the signatures of sunlit and shaded background will also be heterogeneous, due to similar effects.

In practice, however, these simplifications are not always limiting. In real vegetation covers, especially those of low and intermediate densities, the variation between signatures of sunlit and shadowed, crown and background components is usually much greater than the variation within signatures of these components. Further, if the vegetation is strongly absorbing, as is the case in visible portions of the spectrum, the effects of multiple scattering will be further lessened. Therefore, we may expect that a geometric-optical model alone will still be quite useful as a first-order approximation that is able to explain the major portion of variance in the BRDF of a forest, woodland or shrubland.

In our previously published work on geometric-optical modeling of forest reflectance, a problem has arisen when either or both illumination or viewing directions assume large zenith angles. At such angles, the tops of the trees are more likely to be illuminated and visible than the lower portions, and thus the scene will appear brighter than a model simply based on random shadowing would predict. This gives the BRDF a "bowl-shape," in which the reflectance increases for a given sun angle as the observer descends to a position low on the horizon [22]. We refer to this as the "mutual-shadowing problem," since it arises because of the mutual shadowing and obscuring of crowns by one another.

Although in our earlier paper [18] we developed an empirical correction for the mutual-shadowing effect, a primary objective of this paper is to improve this treatment so that it properly reflects the geometry and count-density of the objects. Further, our treatment here is developed for the spheroid as the basic crown shape, which makes it much more generally applicable than the cone shape used in the former paper. We also include a new approximation for the ellipse overlap function, which controls the shape of the hotspot by determining the shadow area of a crown that is not obscured by the crown from a particular viewpoint. As before, we neglect the nonuniformity of component signatures due to multiple scattering effects, and further assume the components to be Lambertian. And, for the purpose of better understanding the geometric-optical effects, we will, for now, assume zero reflectance for shaded canopy and background.

II. Description of Model

A. General Reflectance Model

In Li and Strahler [18], the BRDF of a pixel is modeled as the limit of its directional reflectance factor $R(i, v)$:

$$R(i,v) = \frac{\int\int_A R(s) < i,s > < v,s > I_i(s) I_v(s) ds}{A \cos\theta_i \theta_v} \quad (1)$$

where ds is a small Lambertian surface element over area A of a pixel; $R(s)$ is the reflectance of ds; i, v, and s represent the directions of illumination, viewing, and the normal to a surface element, respectively; $< ., . >$ is the cosine of the phase angle between two directions; θ is the zenith angle of a direction; $I_i(s)$ and $I_v(s)$ are indicator functions, equal to one if ds is illuminated (I_i) or viewed (I_v), zero otherwise. Here the double integral shows that ds is integrated over the pixel—i.e., the footprint of the sensor's field of view.

In order to further the analysis, let's assume that there are only two kinds of surfaces over A—background surface and crown surface—which have Lambertian reflectance G and C, respectively. We may then write (1) as

$$R(i,v) = K_g G + \frac{C}{A} \int\int_{A_c} \frac{< i,s >}{\cos\theta_i} \frac{< v,s >}{\cos\theta_v} ds \quad (2)$$

where $K_g = A_g/A$ is the proportion of background both illuminated and viewed. This equation has a very clear physical meaning. Considering that the union of A_g and A_c is the intersection of the set of surface elements that are illuminated and the set of those that are viewed, only when v and i coincide can A_g and A_c achieve a maximum, provided that the surface elements have no special orientation preference. Thus, the hotspot is well explained by this equation. Another obvious and important meaning of this equation is that the directional reflectance of a scene depends not only on the material reflectance (related to G and C) but also on its spatial structure (which determines A_g and A_c).

For our discussion, it will be helpful to focus on the two terms of (2). The first term describes how the sunlit background proportion proceeds to a maximum as viewing and illumination positions in the hemisphere coincide, and the

second describes how the sunlit crown surface, composed of Lambertian facets, similarly becomes maximally exposed to view at the hotspot, and those facets on tops become dominant at large viewing zenith angles.

B. K_g and the Overlap Function for Crowns

Now, let's analyze how the first term K_gG varies with illumination and viewing geometry. As in Strahler and Jupp [21], we assume that the crowns have the shape of a spheroid, with vertical half-axis equal to b, horizontal radius equal to R, and height to the center of the spheroid h. To accommodate the spheroidal shape easily in the derivations of shadow areas that follow, we will use the transformation $\theta' = \tan^{-1}(\frac{b}{R}\tan\theta)$; this simply replaces θ by the angle that would generate the same shadow area for a sphere. For simplicity, we will assume for now that the centers of the spheroids are randomly distributed in depth from h_1 to h_2 over A. We will also assume that G and C are constant as average signatures over A_g and A_c, so that the problem is to properly model K_g and $K_c = A_c/A$.

In (2), K_g can be expressed easily using the Boolean model [21]:

$$K_g = e^{-\lambda\pi R^2[\sec\theta_i' + \sec\theta_v' - \overline{O}(\theta_i,\theta_v,\phi)]} \tag{3}$$

where $\overline{O}(\theta_i,\theta_v,\phi)$ is the average of the overlap function $O(\theta_i,\theta_v,\phi,h)$ between illumination and viewing shadows of individual crowns as projected onto the background. Here, ϕ is the difference in azimuth angle between viewing and illumination positions.

To simplify the problem, Strahler and Jupp [21] approximate the overlap function by the overlap area of two disks with the original areas and center positions of the two ellipses. This approximation is justified when solar zenith and viewing zenith angles are not too large. In the case of long ellipsoidal shadows, however, this approximation will overestimate the width of the hotspot in the azimuthal direction and underestimate it in zenithal direction. To improve the accuracy and preserve the proper hotspot width information, we have developed another approximation as follows.

Case 1: $\phi = 0$ or $\phi = \pi$ First we consider the overlap function in the principal plane. When $\phi = 0$ or π (i.e., viewer is on the other side of the target from the sun), the elliptical illumination and viewing shadows will be aligned in the same direction. The overlap area is approximated by an ellipse with one axis equal to the overlap length and the other equal to the crown width, yielding

$$O(\theta_i,\theta_v,\phi) = \frac{1}{2}\left[\sec\theta_i' + \sec\theta_v' - \frac{h}{b}|\tan\theta_i' - \tan\theta_v'\cos\phi|\right]. \tag{4}$$

When the overlap area goes to zero, the hotspot effect disappears. Thus, the shape of the hotspot function, that is, the way in which it falls off as viewing and illumination positions diverge, will be conditioned primarily by the shape and height of the spheroids.

Equation (4) is helpful for us to understand how the shape of crowns governs the shape of overlap function, and is a good approximation in usual cases. In a case where it is important to have an exact solution for overlap function on the principal plane, we have proven:

$$O(\theta_i',\theta_v',\phi) = (t - \sin t\cos t)\,(\sec\theta_i' + \sec\theta_v')/\pi \tag{5}$$

where

$$\cos t = \frac{h|\tan\theta_i' - \tan\theta_v'\cos\phi|}{b(\sec\theta_i' + \sec\theta_v')}. \tag{6}$$

We have also obtained exact overlap function on the principal cone, i.e., where $\theta_v' = \theta_i'$ and ϕ varies from 0 to 2π. However, since (4) is accurate enough for our purpose in this paper and conceptually simpler, we will keep using it in the later text.

Case 2: $\phi \neq 0,\pi$ and $\theta_i \neq \theta_v$ Here we assume that the viewing zenith is still θ_v, but the viewing direction has a different azimuth than the illumination position. Rather than compute the overlap of two ellipses at arbitrary inclinations and distances directly, the strategy will be to fit a linear function to the diminution of overlap with azimuth angle. We approximate

$$\Phi = \frac{4R}{h(\tan\theta_v + \tan\theta_i)} \tag{7}$$

as the azimuthal cutoff of the hotspot; and linearly interpolate for ϕ between 0 and Φ or π, whichever is smaller. For the case $\Phi < \pi$, we will assign $O(\theta_i,\theta_v,\phi) = O(\theta_i,\theta_v,\phi = \pi)$ for all ϕ between Φ and π. Though the above approximation may produce small errors in the overlap area, the basic and clear causal relation between the canopy structure and the hotspot is preserved. Monte Carlo simulation shows that the above approximation is very close to simulated results for a wide range of solar zenith angles and crown shapes, giving accurate delineation at the edges of the hotspot (which is of special interest here).

From (4), we may conclude that (1) the azimuthal width of hotspot effect is basically determined by R/h ratio; (2) the outward width of hotspot on the principal plane is determined by b/h ratio; and (3) the inward width is determined by both.

C. Contribution of Sunlit Canopy Surface and Effect of Mutual Shading

Here we model the effect of sunlit canopy on the bidirectional reflectance (second term in (2)). This variation is more difficult to deal with, for it depends on the both the density and angular distribution of ds in (2). For simplicity, Strahler and Jupp (1990) assumed that each crown could be modeled as a sphere without mutual illumination shading between ds elements. Then the second term can be approximated as:

$$K_cC = \frac{1}{2}(1 + < i,v >)(1 - e^{-\lambda\pi R''^2\sec\theta_v})C \tag{8}$$

In this expression, the first term is the illuminated proportion of the area of a single sphere viewed at position v and illuminated at position i. This is weighted by the second term, which is the proportion of the area of spheres visible from zenith angle θ_v. Since both terms vary smoothly between zero and one,

this contribution to the hotspot is quite flat. In the case of a spheroid, we can simply replace $< i, v >$ by $< i', v' >$, where

$$< i', v' >= \cos\theta_i' \cos\theta_v' + \sin\theta_i' \sin\theta_v' \cos\phi. \quad (9)$$

The first term in (8) ignores the problem of mutual shading of one canopy by another. Strahler and Jupp [21] handle this problem by multiple integration, in which the mutual shadowing of canopies by one another is treated in the same way as the mutual shading of leaves by one another, but our objective here is to derive a simple approximation to describe the effect for vegetation covers composed of collections of individual, discrete canopies. To carry this out, we have developed an approach that applies one-stage geometric optics to deal with the spatial relationship between the part of the crown surface that is mutually shaded in the illumination direction and the part mutually shaded in the view direction. That is, when the shapes are large relative to the thickness through which their centers are distributed, these shadows will tend to shade or obscure the lower portions of the shapes preferentially.

D. Mutual Shadowing Proportions

In [17] and [23], we proved by simulation and mathematics (simplified to the one-dimensional case) that for the nadir-viewed cone model, mutual shadowing of illumination will not change the ratio $K_c/(1 - K_g)$. (This ratio was itself denoted K_c in [17], but since then we have turned to the use of K_c as A_c/A for consistency with K_g in subsequent publications.) Although this is a helpful result, it holds only for the case of nadir viewing of cones, or more generally for the cases where the mutual shadowing in illumination and viewing directions is independent.

For the more general case, let's first consider the proportion of crown surface that will be mutually shadowed by other crowns. In the direction of illumination, each crown has an area $\pi R^2 \sec\theta_i'$ projected onto the ground, and the total projected area (as a proportion of A) then will be $\lambda\pi R^2 \sec\theta_i'$, if there is no mutual shadowing. Because of mutual shadowing, however, the net projected area will be $1 - e^{\lambda\pi R^2 \sec\theta_i'}$. The difference therefore will indicate the total mutual shadowing. Thus, we may define the quantity M_i, the mutual shadowing proportion in the illumination direction, as

$$M_i = 1 - \frac{1 - e^{-\lambda\pi R^2 \sec\theta_i'}}{\lambda\pi R^2 \sec\theta_i'}. \quad (10)$$

M_i will therefore be an index showing the degree of mutual shadowing in the illumination direction. In other words, each spheroid will, on average, have a proportion M_i of its ground-projected area that will not be sunlit. Let's assume that this part will be concentrated at the lower part of the spheroid. We may then imagine a boundary drawn on the surface of the spheroid with the area comprising M_i located below it (Fig. 1). Similarly, we can define M_v as the mutual shadowing proportion in the view direction as

$$M_v = 1 - \frac{1 - e^{-\lambda\pi R^2 \sec\theta_v'}}{\lambda\pi R^2 \sec\theta_v'}. \quad (11)$$

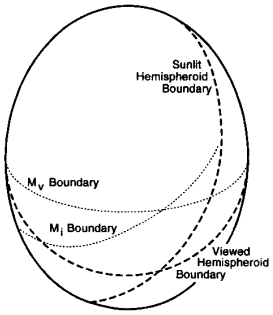

Fig. 1. Diagram showing M_i and M_v for a spheroid.

If we again assume that viewing shadows are concentrated at the lower part of the spheroid, we can similarly define a M_v boundary (Fig. 1).

Clearly, the proportion of sunlit crown the sensor can see (corresponding to the area above both M_i and M_v boundaries) depends on both zenith and azimuth differences between the illumination and view directions. At the hotspot, M_i and M_v boundaries will overlap and the the sensor will see no mutual shadowing. When the view zenith angle is larger than the illumination zenith angle, M_v will be greater and M_i, and little or no mutually-shaded crown will be visible, depending on the azimuth difference. When the reverse is true, mutual shadows will be visible. Thus, this simplification captures the essence of the mutual-shading effect. However, the true situation is that the mutual shadowing won't be strictly under the M_i or M_v boundaries, even the crown centers are uniformly located at the same height. But for now, we will make this assumption and discuss its implications later.

E. The f-Ratio of Nonnadir-Viewed Spheroids

For the spheroidal case, it is necessary to show whether the f-ratio will be still independent of density, as in the case of the nadir-viewing cones [17], [23]. First we consider a single spheroid in a pixel. From the view direction, the spheroid will have a projected area $\Gamma_v = \pi R^2 \sec\theta_v'$; however, only the portion $\frac{1}{2}(1+ < i', v' >)$ of that area will be sunlit. Similarly, the illumination shadow on the ground will occupy the area $\pi R^2 \sec\theta_i'$. The compound area of viewed crown plus illumination shadow (again as projected onto the background) will be $\Gamma = \pi R^2 [\sec\theta_i' + \sec\theta_v' - O(\theta_i', \theta_v', \phi)]$. Thus, we define the ratio F for a single spheroidal crown as

$$F = \frac{\Gamma_c}{\Gamma} = \frac{\frac{1}{2}(1+ < i', v' >)\sec\theta_v'}{\sec\theta_i' + sec\theta_v' - O(\theta_i', \theta_v', \phi)}, \quad (12)$$

where Γ_c is the sunlit area of the crown, and we define the corresponding ratio

$$f = \frac{K_c}{1 - K_g} \quad (13)$$

for a pixel or a scene. It is easy to show that in the case of an one-crown pixel, $f = F$.

Now let's imagine that there are n such crowns and shadows within a pixel. If there is no mutual shadowing, we still have

$f = F$. As n increases, however, mutual shadowing will likely begin, and $K_g = e^{-\lambda\pi R^2[\sec\theta_i' + \sec\theta_v' - \bar{O}(\theta_i,\theta_v,\phi)]}$ will be the mean of the random case. Similar to (10), we define the mutual shadowing proportion M as

$$M = 1 - \frac{1 - K_g}{\lambda\Gamma}, \tag{14}$$

which is the fraction of total shadowing cast from single crowns that falls on other crowns instead of the background.

The sunlit and viewed crown surface of any single crown will be reduced by hiding either from viewing or from illumination. Thus, the f-ratio with mutual shadowing will be

$$f = \frac{n\Gamma_c - \sum \Delta_{A_c}}{A(1 - K_g)}, \quad = F\frac{1 - \sum \Delta_{A_c}/(n\Gamma_c)}{1 - M} \tag{15}$$

where $\sum \Delta_{A_c}$ is total decrement from $n\Gamma_c$ to A_c, i.e., the background-projected area of viewed sunlit crown surface. We may express $\sum \Delta_{A_c}$ as three terms: a decrement due to mutual shading in the view direction, plus a decrement due to mutual shading in the sun direction, minus those elements shaded in both directions:

$$\sum \Delta_{A_c} = n\Gamma_v(P_v M_v + P_i M_i - P_o), \tag{16}$$

where P_v is the conditional probability that a crown surface element will face the sun given that it is mutually shaded from view; and P_i is the probability that a crown surface element will face the viewer given that it is mutually shaded from illumination. Both P_i and P_v are average proportions of areas projected in the view direction.

P_o, the third term, is the overlapped part of the first two terms, expressed as a fraction of Γ_v. P_o contains three parts, derived from three types of surface elements. First are those surface elements involved in the intersection of crowns. These will always fall inside other crowns, and thus will contribute to neither the hotspot nor to the bowl shape of the BRDF. Second are those surface elements that fall within overlapped illumination and viewing shadows of another single crown. This collection obviously contributes to the hotspot, and is due to the spatial correlation of the shadows. Third are those surface elements that fall into one crown's illumination shadow but in another crown's viewing shadow. These elements will contribute to the top-crown viewing phenomenon, which occurs when the probabilities of being hidden in two directions are not independent.

Substituting (16) into (15) yields a single expression for f

$$f = F\frac{1 - \Gamma_v(P_v M_v + P_i M_i - P_o)/\Gamma_c}{1 - M}. \tag{17}$$

F. Modeling P_v, P_i and P_o in the Principal Plane

Now, our problem is to model these three P's. However, we prefer at present to treat these three parts at the same time by assuming two extreme cases:

1) ("Uniform Height") All illumination or viewing shadows are under M_i or M_v boundaries respectively, and the intersection and hotspot contribution part will be naturally included in the intersection of these boundaries.
2) ("Random") Illumination and viewing shadows are independently scattered on other crowns, thus both the hotspot and bowl-shape contribution of mutual shadowing can be ignored.

In the first case, refer to Fig. 1 to model P_v, P_i and P_o, where an "average crown" is used to visualize the M_v and M_i boundaries. If viewing and illumination shadows fall strictly below M_v and M_i boundaries, then P_v, the conditional probability that a crown surface element will face the sun given that is it mutually shaded from view, will be the ratio of the illuminated portion of the projected surface below the M_v boundary to the total projected surface below the M_v boundary. Correspondingly, P_i, the conditional probability that a crown surface element will face the viewer given that is it mutually shaded from illumination, will be the ratio of the viewed portion of the projected surface area below the M_i boundary to the total area below the M_i boundary (not completely shown in Fig. 1). Note that M_i is the proportion of mutually-shaded crown surface projected to the direction of illumination, but $P_i M_i \Gamma_v$ is the area of this fraction of crown surface projected to viewing direction. Thus proper calculation of these areas will involve some projection change. P_o is the overlap area of these two, represented as a fraction of Γ_v.

Let's first consider the case in the principal plane, which is shown in the four parts of Fig. 2. For simplicity, we will assume that all shadows fall below the boundaries M_v and M_i, which are the traces of planes intersecting the spheroid at its center ("great ellipses"). The angle between the planes of the M_i great ellipse and the illumination boundary (which is also a great ellipse) is:

$$\theta_{M_i} = \cos^{-1}(1 - 2M_i). \tag{18}$$

We define θ_{M_v} similarly. At the hotspot, the M_i and M_v boundaries coincide Fig. 2(a), and thus $P_v = P_i = 1$, $P_o = M_v = M$, and $f = F = 1$.

Now, assume that the viewing zenith angle increases to $\theta_v > \theta_i$. In usual cases when mutual shadowing on crowns is to be considered, the M_v boundary is higher than the M_i boundary. The sensor's view is shown in Fig. 2(b), where P_v is the ratio of the area between M_v boundary and the illumination boundary to the whole area under the M_v boundary. That is,

$$P_v = \frac{M_v\Gamma_v - (\Gamma_v - \Gamma_c)}{M_v\Gamma_v}, \tag{19}$$

while P_i is always one, and P_o always cancels the M_i term. Then, (17) becomes

$$f = F\frac{1 - P_v M_v \Gamma_v/\Gamma_c}{1 - M} = F\frac{(1 - M_v)\Gamma_v}{(1 - M)\Gamma_c} = \frac{1 - e^{-\lambda\Gamma_v}}{(1 - K_g)} \tag{20}$$

This result tells us that when the viewing direction in the principal plane deviates from hotspot outward ($\theta_v > \theta_i$), the f-ratio will change little from one if coverage is high and θ_v is large, reflecting the fact that almost no shadows on crowns can be seen.

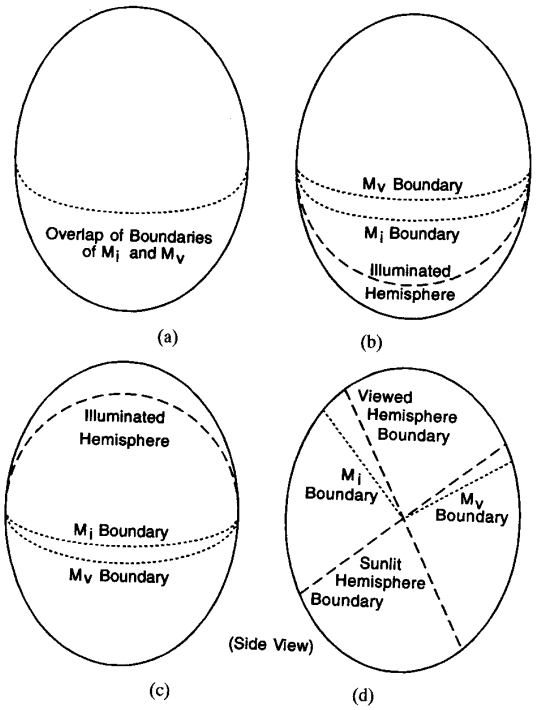

Fig. 2. Various views of a spheroid illustrating mutual shadowing when illumination and viewing positions are in the same azimuthal plane. A, at the hotspot. B, $\theta_v > \theta_i$. C, $\theta_v < \theta_i$. D, θ_v and θ_i on opposite sides of nadir, with view from the side.

When the sun is close to nadir and the coverage is very low, the increment of θ_{M_v} may be so small that M_v will be under the M_i boundary. In this case, mutual shadowing can be simply ignored as in [21].

When θ_v moves inward from the hotspot on the principal plane (but has not reached nadir yet), an average crown will look like Fig. 2(c), where we assume M_i is higher than M_v. Hence, $P_v = 1$, $P_o = M_v$, and

$$P_i = \frac{1 - \cos(\theta_{M_i} - \theta_i' + \theta_v' \cos\phi)}{1 - cos\theta_{M_i}}, \tag{21}$$

or zero, if the M_i boundary is too low to show up in sensor's view.

After θ_v passes the nadir, the M_v boundary goes to the opposite side of the spheroid from M_i. In this case, the average crown the sensor sees will resemble Fig. 2(d), which shows the horizontal projection of an average crown at $\phi = \pi/2$ so that we can identify all boundaries clearly. For this case, P_i is the same as in (21), and with ϕ equal to π. P_v is the fraction of M_v over the illumination boundary, i.e.,

$$P_v = \begin{cases} \frac{1-\cos(\theta_{M_v} - \theta_v' + \theta_v' \cos\theta)}{1-\cos\theta_{M_v}}, & (\theta_{M_v} - \theta_i' + \theta_v' \cos\theta) \geq 0 \\ 0, & (\theta_{M_v} - \theta_i' + \theta_v' \cos\theta) < 0 \end{cases} \tag{22}$$

Note that when θ_v is between the hotspot and nadir, P_v is always one, and thus a discontinuity of P_v appears at the nadir. This discontinuity arises from the assumption that all shadows fall under the M_v boundary, and when viewing the direction passes nadir, there is a sudden change for viewing shadows from the same side of crown as the illumination shadow to the opposite side of the crown. The discontinuity of P_v reflects this fact. Monte Carlo simulation, discussed in a later section, shows the same pattern when the crowns are distributed at the same height. However, as we stated previously, in such cases, all M_v at $\theta_v = 0$ is owing to physical intersection of crowns, and such intersection will not change with viewing geometry, thus $P_v M_v$ should be still continuous at nadir, and equal to P_o in fact. In other words, the formula for Case 2 will be extended to the Cases 3 till very large viewing zenith, so that $\theta_{M_v} - \theta_i' + \theta_v' cos\phi) > 0$ again.

In the "random" case, M_i and M_v are independent and thus $\sum \Delta_{A_c}/(n\Gamma_c) = M$, so (15) simplifies to $F = f$. But the practical situation is always between these two extremes, depending upon the height distribution. If all the crowns are at the same height, the situation will be very close to the "uniform height case"—the mutual shadows will always fall on the lower part of the crowns and thus the crown top-viewing effect will be strong. However, when tree heights are distributed over a wide range, the top layer of the forest canopy will play a more important role in determining the BRDF of the canopy than the lower layer. Therefore, we cannot say that when crown heights are distributed in a wide range, the bowl-shape of the BRDF will not be apparent; rather, it will be determined basically by size, shape, and height of crowns in the top layer. Thus, we presently restrict ourselves to considering a single top layer only, where the range of distribution of height does not exceed twice the vertical axis of the spheroid. At such an intermediate height distribution range, we will take a weighted average of the two values associated with each extreme.

To share the weighting between the two cases, we use the parameter

$$\beta = \left(1 - \frac{h_2 - h_1}{4b}\right)^2, \quad \text{if}(h_2 - h_1) \leq 4b. \tag{23}$$

When $(h_2 - h_1) > b$, β is forced to be zero, indicating the "random" case, or, better to say, we have to redefine the layers. Then both P_v and P_i are calculated as a weighted sum of corresponding terms

$$P = \beta P_1 + (1 - \beta) P_2, \tag{24}$$

where P_1 and P_2 are the probabilities associated with Cases 1 (uniform height) and 2 (random) above.

Fig. 3 shows values for P_i and P_v calculated in the principal plane using the formulae above. The calculations use a density of 30 crowns of 3-m radius per 900 m^2 area, a crown shape ratio $b/R = 1.5$, $b/h = 0.18$, and a canopy height $h = 25$m. Vertical coverage for this example is $1 - e^{-\lambda\pi R^2} = 0.61$. The illumination zenith angle is taken as $\theta_i = 30°$. Note that the horizontal axis is plotted as θ_v' rather than θ_v; for this shape, $\theta_v = 30°$ gives $\theta_v' = 40.9°$. In Fig. 3(a), $h_2 = h_1 = h$; in B, $(h_2 - h_1)/h = 0.2$; and in C, $(h_2 - h_1)/h = 0.4$; that is, $\beta =$ 1, 0.53, and 0.20, respectively.

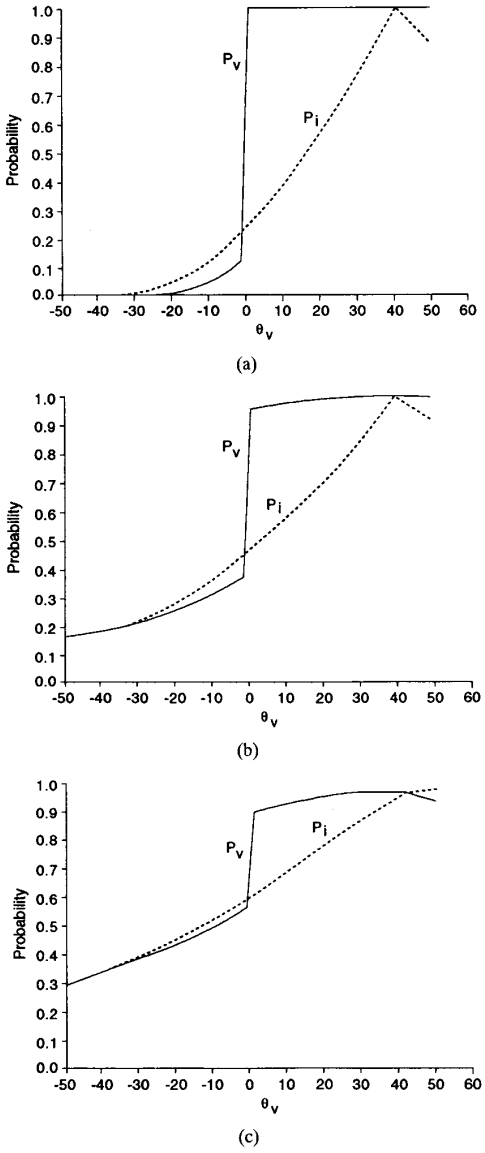

Fig. 3. Calculated values for P_i and P_v using formulas (21)–(24). Parameters as described in text.

G. Validation Using Monte Carlo Simulation

To validate these approximations, we developed a Monte Carlo simulation program to evaluate P_i, P_v, P_o and M for the spheroidal crown model. It first generates 3-D random locations of centers of spheroids according to the given parameters. Then it calculates and stores the area, location, and orientation of flat surface elements conforming to the surfaces of each spheroid using a given step size in a spherical coordinate system originated at the center of the crown. This accomplished, the program calculates the surface normal of each element, and if the dot-product of its normal and illumination direction is negative, the element is classified as an element "facing away from the sun." Otherwise, the program calculates whether it is in the illumination shadow of any other crown. Border effects are handled by projecting the shadows of the far edge to the near edge. If an element is not in any shadow, it is classified as a sunlit element; if it falls within the shadow of any other crown, it is a "mutually shaded" element. However, if the element itself falls inside another crown, as when two or more crowns intersect, it is classified as an element facing away from the sun in order to reduce the number of categories. (The percentage of these concealed elements is easy to retrieve, since the percentage of real "facing-away" elements is always 50%.) Then a similar procedure repeats for each viewing direction, yielding a total of nine categories of surface elements. Finally, the total areas of surface elements in each class for each given illumination and viewing position are summed, and the totals and appropriate proportions are output for further analysis. The procedure may be repeated for different random draws of spheroid center points.

Figs. 4(a–c) present P_v and P_i values obtained from simulation, with the same scene parameters as Figs. 3(a–c). It is obvious that the calculated results catch the basic features of the simulation reasonably well. There are also some noteworthy differences between simulated and calculated results, especially between Fig. 3(a) and Fig. 4(a). After passing the nadir, the calculated P_v drops from one to about 0.1 instead of to zero as in the simulation. This is because the simulation properly ignores the intersected crown elements, whereas the calculation shows θ_{M_v} larger than θ_i, and thus part of the surface that is mutually shaded from view still faces the sun. These elements are indeed those of intersected crown surfaces, since the crown centers are distributed at the same height. When the viewing zenith angle increases from nadir, the calculated P_v remains flat, but the simulated P_v starts to increase slightly at about $-10°$. This increase occurs when θ_{M_v} finally increases faster than θ_v. Then, the M_v boundary goes up again above the illumination boundary, which should occur at about $\theta'_v < -75°$. This difference reflects the fact that viewing shadows are not strictly under the M_v boundary even when all crowns are centered at the same height. But as we can predict, this difference will not yield a large error in the BRDF calculation. We also have carried out a further series of comparisons of calculated and simulated values for P_i and P_v with varying densities and sizes, and the results are largely similar, thus validating the computational approach as a reasonable approximation.

H. Azimuthal Variation

Figs. 3 and 4 display results in the principal plane. Let us now turn to variation induced by change in relative azimuth. For this discussion, we will define the "principal cone" as the azimuthal cone in which θ_i is fixed and ϕ varies. First, consider the geometry involved. Fig. 5 presents a horizontal projection of an average crown in the direction of the viewing azimuth for a situation in which $\phi \neq 0$. In this case, P_v is proportional to the spherical triangle ABC, P_i is proportional to DEF, and P_o is their intersection ABGD. Even in this simple case, calculating these values will be tedious, but it is easy

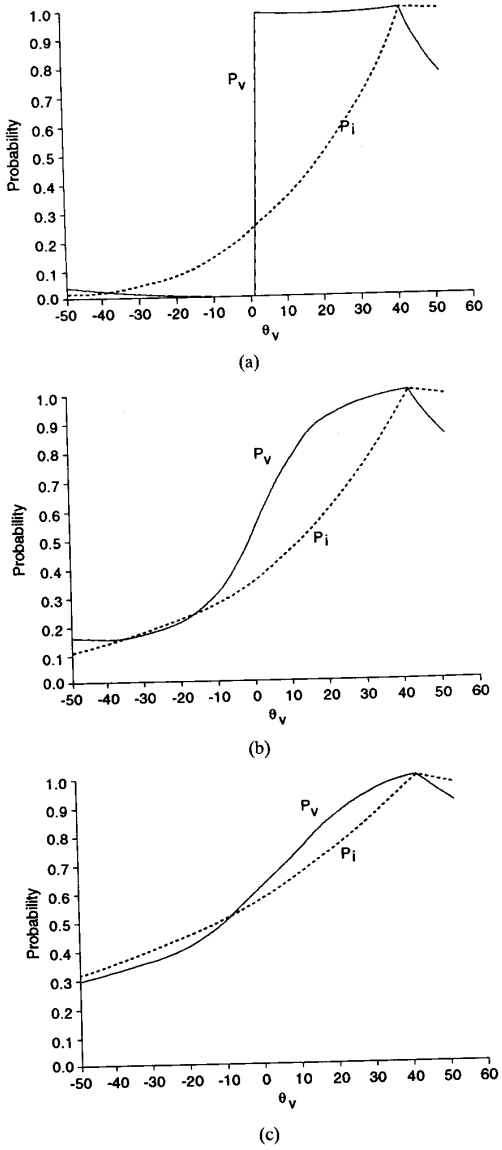

Fig. 4. Values for P_i and P_v using Monte Carlo simulation. Parameters as described in text.

to imagine that as ϕ gets larger and larger, the illumination boundary (the arc FADC) will move leftward, and thus P_v, P_i, and P_o will all shrink, going to zero at the antihotspot direction ($\phi = \pi$) (assuming that M_v remains below the illumination boundary). This relation can be fairly approximated as being linear and applicable to other θ_v angles also.

Thus, knowing the values of P_v, P_i, and P_o for given θ_i, θ_v on the principal plane ($\phi = 0, \pi$), it is not difficult to obtain the f-values for other ϕ by interpolating the P_v, P_i, and P_o at any ϕ. Of course, they may also be calculated more accurately by spherical surface geometry. At present, we may expect that a linear or negative exponential approximation will be simple but accurate enough. Figs. 6(a–c) show how P_v

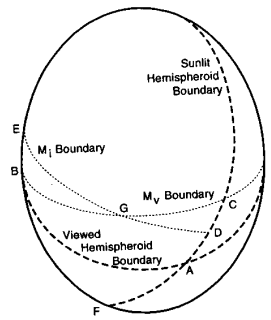

Fig. 5. Diagram of a circular crown viewed horizontally in the direction of viewing azimuth with illumination azimuth to the observer's left.

and P_i values obtained from simulation vary on the principal cone, using the same canopy parameters as those in 3(a–c), respectively. As in the case of variation along the principal plane, the approximation captures the variation quite well.

In short, our examination of the mutual shadowing of crown surfaces yields a simple approach to modeling the bowl-shape of the BRDF—changing (8) to

$$K_c C = (1 - K_g) f C, \tag{25}$$

in which f is calculated at $\phi = 0, \pi$ for the principal plane case from (23), using (17) and (24), and then interpolated to the proper azimuth.

III. Forward Simulation of BRDF's

To explore this model more fully, we calculated a number of BRDF's for several sets of geometric parameters and illumination angles. In selecting the parameters, we tried to choose reasonable values for three vegetation covers—conifer forest, savanna, and shrubland—at plausible cover percentages, solar zenith angles, and in typical reflectance bands. Three basic shapes of spheroids were used (Table I). Conifer forest was modeled as a collection of spheroidal crowns, 6 m wide and 20 m tall, with a maximum height to the top of the crown of 30 m. For savanna, our tree shape was a flattened spheroid, 10 m wide and 5 m high, with a maximum height of 15 m. For the third cover type, shrubland, the shrub was taken to be a spheroid 0.5 m wide, 1 m high, and resting on the ground. For each vegetation type, we also selected low and high percent cover values that we thought might be typical of real values. The cover value is simply the random expectation of crown cover at nadir, i.e., $1 - e^{-\lambda \pi R^2}$. These are provided in the table as well.

In exploring modeled BRDF's for these vegetation covers, two sun angles were chosen—15° and 55°. These seemed realistic for a satellite-sensing scenario that would include overpasses from midmorning to midafternoon at all seasons of the year. For spectral bands, recall that in the general geometric-optical model, there are four scene components: sunlit and shaded canopy (or leaf), and sunlit and shaded background, and that the proportions of the four scene components as a function of view and illumination positions are weighted by their radiance or reflectance signatures to provide

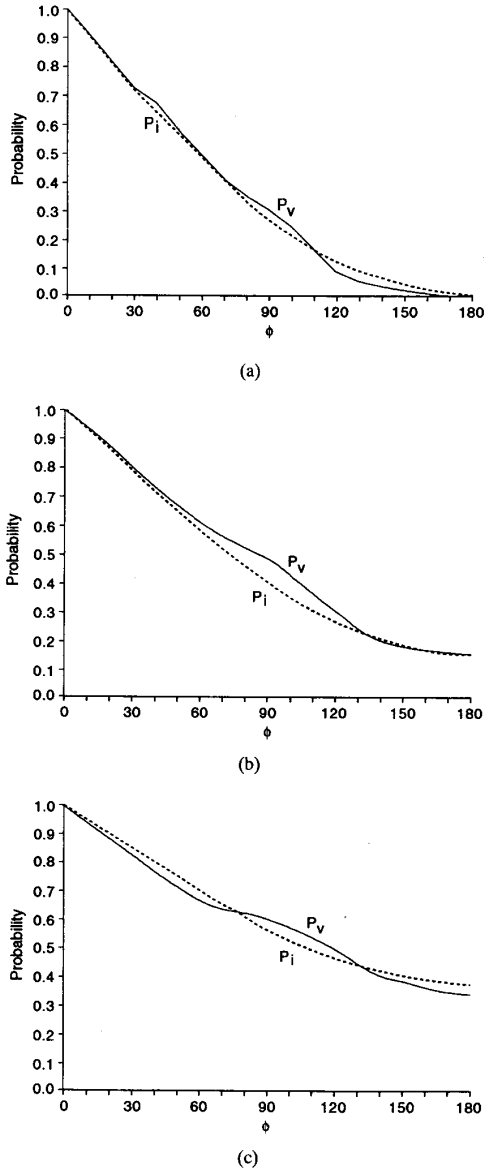

Fig. 6. Values for P_i and P_v in the principal cone using Monte Carlo simulation. Parameters as described in text.

TABLE I
SHAPE AND COVER PARAMETER SETS

Cover Type	b, m	h, m	R, m	Cover, Percent Low	Cover, Percent High
Conifer	10	20	3	20	60
Savanna	2.5	12.5	5	10	40
Shrub	0.5	0.5	0.25	30	80

the radiance or reflectance of the scene as a whole. In the mutual-shadowing model derived above, we have considered two components only—sunlit crown (C) and sunlit background (G)—but since the random expectation of total ground and crown cover at any view angle is so easily determined, the calculation of the proportion of the scene in shaded components is quite simple. However, to reduce complexity somewhat, we considered shaded canopy and shaded background to have the same reflectance signature (Z), resulting in a three-component model. Two bands were considered: red and near-infrared (Table II). Although the values selected are generally typical of reflectances observed in these regions for plant matter and soil, their main significance lies in the fact that for the red band, the sunlit crown is darker than sunlit background, whereas, in the near-infrared case, sunlit crown is lighter. Thus, red–near-infrared comparisons help clarify the role of the relative brightness of the two cover types in controlling the shape of the BRDF.

TABLE II
REFLECTANCE VALUES FOR SCENE COMPONENTS

Band	G	C	Z, T
Red	0.15	0.08	0.01
Near-Infrared	0.20	0.55	0.05

In the figures that follow, the BRDF's are displayed in a rectangular coordinate system. Each viewing position in the hemisphere is taken as as a pair of polar coordinates, resolved onto the x-y plane as a vector of unit length, and the reflectance at that position is taken as the z-value. This produces a three-dimensional surface which is then displayed as if viewed from "behind" and above. (For ease in discussing the shapes of the BRDF's we will regard viewing positions near the principal plane on the hotspot side as the "front" of the BRDF and viewing positions near the principal plane opposite the hotspot as the "back.")

A. BRDF's Without Mutual Shading

The BRDF of a vegetation cover is a complex function of a set of variables, including the shape of the crown, the range of heights through which crown centers are distributed, the count density of crowns on the surface, and the spectral band in which measurements are made. To better understand the effects of each, we will examine the basic features of BRDF's before and after the effects of mutual shading are accommodated. We begin with a discussion of BRDF's for which mutual shading is nearly absent—that is, the parameter β is set to 0.05, indicating that the probabilities of view and illumination for any crown surface facet are nearly independent.

1) Effect of Crown Shape and Spectral Band on the BRDF Fig. 7 presents six modeled BRDF's for the three basic spheroid shapes as calculated for red and near-infrared bands.

Each type is at high cover and illuminated at a 55° solar zenith angle. As the figure shows, each spheroid generates a differently-shaped hotspot. Since the conifer is a tall, thin ellipsoid, its hotspot is much wider (in an angular sense) in the zenithal direction than in the azimuthal direction. This assymetry occurs because a greater area of shadow behind the crown is revealed for a given change of view angle in the direction of the principal cone than in the direction of the principal plane. The savanna shape shows the opposite characteristic—a hotspot that is wider in the

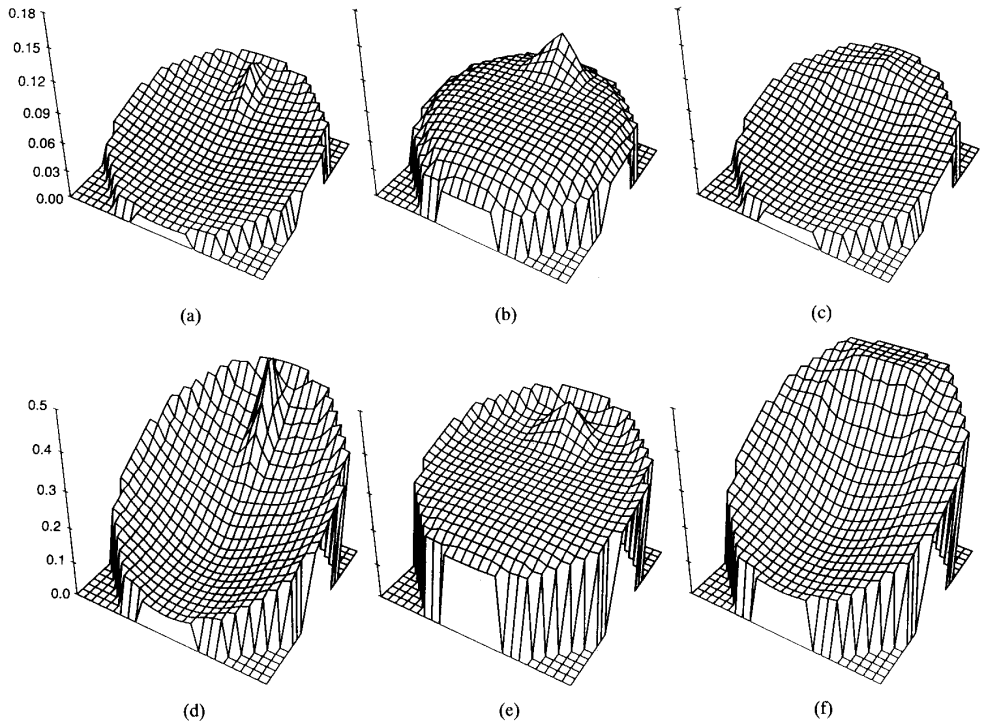

Fig. 7. BRDF's in the red (a–c) and near-infrared (d–f) bands for conifer (a, d), savanna (b, e), and shrubland (c, f) vegetation types at high cover and 55° solar zenith angle. Mutual shadowing is set at a very low value ($\beta = 0.05$) to emphasize the effect of geometric shape.

azimuthal direction than in the zenithal direction. This results from a similar effect in the opposite direction, in which the shadow is revealed more quickly in the zenithal direction than in the azimuthal direction. The shrub shape presents the broadest of all hotspots; it is especially broad around the principal cone. This effect occurs because the shrub sits directly on the ground and obscures part of its shadow from almost all viewing positions except those at back of the BRDF.

Beyond the hotspot, the general shape of the BRDF is also of interest. For the conifer and shrub types, the BRDF exhibits a bowl-shape, whereas for the savanna type the shape is more of a dome. In the case of the conifer and shrub, these long shapes present a wider cross section toward the viewer as the viewing position drops toward the horizon and thus they obscure more dark shadows falling on the background within the vegetation stand. However, the savanna trees, being quite broad, present their greatest cross section when the viewer is overhead. As the viewing position descends, their cross section decreases and more dark shadows are visible.

Also of note is the fact that the shapes of the BRDF's of each type are similar for both bands, in spite of the contrast reversal that occurs between canopy and background. Thus, the shape of the BRDF is primarily a function of the geometry of the objects. We do see, however, that the bowl-shape of the conifer and shrub BRDF's is accentuated for the near-infrared. This occurs because the crown cross-section is brighter than the background in the near-infrared, and as the viewer descends from an overhead position, not only are more shadows obscured, but they are also obscured by a brighter canopy material. For the savanna canopy, the same effect flattens the BRDF, but it still maintains a slight overall dome-shape. The general upward slope from back to front for all the BRDF's results because the brightness contribution of the crown always increases as the viewer moves from back to front at the same view zenith, since more and more of the crown will become sunlit as the hotspot azimuth approaches. The very slight upward turn at the edges of the BRDF is produced because β is nonzero and at the largest view zeniths a slight mutual shadowing effect is felt.

2) Effect of Cover on the BRDF Fig. 8 shows BRDF's for the three vegetation types in the red band. For each vegetation type, low and high cover conditions are contrasted. As in the previous figure, mutual shadowing is set at a very low value. As we might deduce from the discussion in the preceding section IIB the cover does not influence the shape of the hotspot, only its height. That is, the hotspot "cutoff" positions on the principal plane and principal cone do not depend on the density of the spheroids, only on their geometry and height above the ground. This phenomenon is obvious from examination of the figure. The cover does, however, influence the overall height of the BRDF. Since the background is brighter than the crowns in the red band, the BRDF with the lower cover is the naturally the lighter.

Beyond the hotspot, the cover does influence the overall shape of the BRDF somewhat. For example, the conifer BRDF changes from a slight bowl-shape to a slight dome when cover is reduced from 60% to 20%. In this case, shaded crown is being revealed slightly more quickly than shaded background

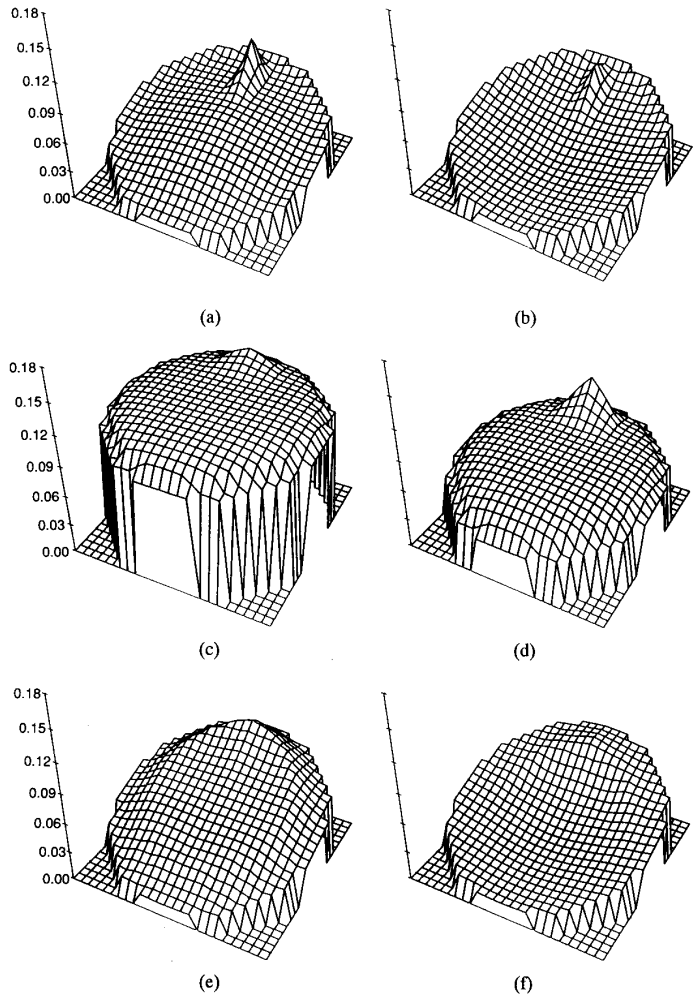

Fig. 8. BRDF's for conifer (a–b), savanna (c–d), and shrubland (e–f) vegetation types in the red band at 55° solar zenith angle. Left (a, c, e): low cover. Right (b, e, f): high cover. Minimal mutual shading.

is being obscured as the observer drops away from the nadir viewpoint. A similar phenomenon flattens the bowl-shape for the shrub canopy at the lower cover value.

3) Effect of Sun Angle on the BRDF A change in sun angle affects the BRDF because it changes the shapes of the shadows that are cast by the plant crowns (Fig. 9). The most obvious change is to the hotspot. As the sun rises in the sky, shadows become smaller and fall closer to the object center. Further, shadows of the spheroidal crowns will tend to become more circular, thus reducing the assymetry of the hotspot in the principal plane and principal cone directions. These effects will tend to broaden the width of the hotspot and make it appear more uniform as its center moves to a new position nearer to nadir. This effect can be easily seen in the figure, which displays near-infrared BRDF's. The same features are evident in red BRDF's (not shown).

Beyond the hotspot, the general shape of the BRDF does not change much. The overall level of reflectance increases somewhat, since the shadows are now smaller. For the shrub case, the modest bowl-shape nearly disappears, although the BRDF is still clearly at a minimum at the back of the function where shadows are not obscured by crowns.

B. Effect of Mutual Shadowing on the BRDF

The approximation to include the effects of mutual shading into the geometric-optical BRDF calculation has the primary effect of deepening the bowl at the back of the BRDF. This is clearly shown in the BRDF's of Fig. 10, where β = 0.0, 0.6, and 1.0 for conifer (red) and savanna (near-infrared) vegetation types at high cover and large solar zenith angle. However, the deepening is actually accomplished by raising the brightness at other view angles, since the effect of mutual shadowing is to obscure the shadows and enhance the amount of crown seen. Thus, the hotspot becomes less distinctive as the effect of mutual shadowing increases. In the conifer case, a strong bowl appears, with a distinct edge corresponding to the viewing position at which M_i falls below M_v. In the savanna case, the

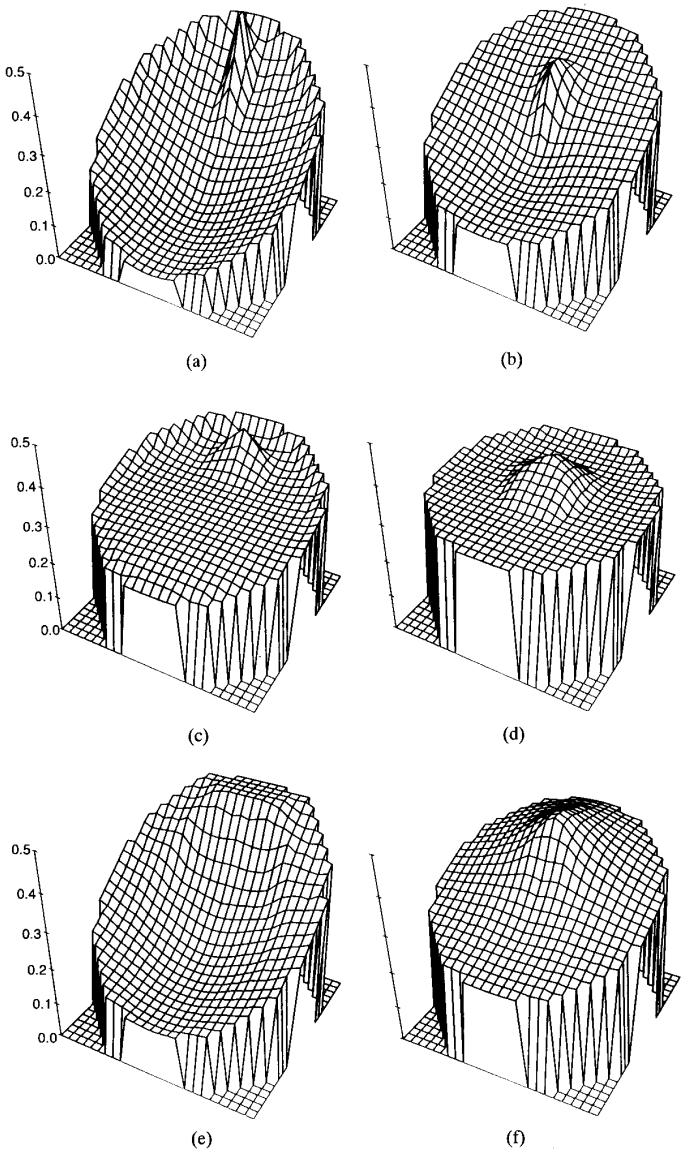

Fig. 9. BRDF's for conifer (a–b), savanna (c–d) and shrubland (e–f) vegetation types in the near-infrared band. Left (a, c, e): Solar zenith angle 55°. Right (b, e, f): Solar zenith angle 15°. Minimal mutual shading.

effect is to turn up the BRDF at the edges, while its modest dome-shape is preserved near the center.

Inspection of the figure suggests that the mutual-shadowing correction has a stronger effect in the near-infrared than in the red. Since the scene proportions are not functions of the spectral band, we may conclude that this effect results simply because the crown reflectance is brighter and the effect simulates the seeing of a greater proportion of crown than expected in the random case. Other plots of BRDF's (not shown) confirm this understanding.

Regarding changes to the BRDF that occur as a function of illumination position, cover, and spectral band while mutual shadowing is accommodated, in general the effects are similar to those that occur without accounting for mutual shading (Fig. 11). With shifting illumination angle, the hotspot moves to the new illumination position and broadens if nearer to nadir, or narrows if further from nadir (Figs. 11(a), (b).) With increasing cover, the effects are generally the same, but with the enhanced bowl-shape superimposed (Figs. 11(c), (d)), compare with Figs. 8(e),(f)). With change in spectral band (Figs. 11(e), (f), compare with Figs. 7(b),(e)), the geometry still dominates, but the stronger mutual shadowing effect in the near-infrared obscures the hotspot to a significant degree.

IV. Discussion

The most obvious feature of the BRDF of vegetation covers that consist of discrete plant crowns is the hotspot. The hotspot

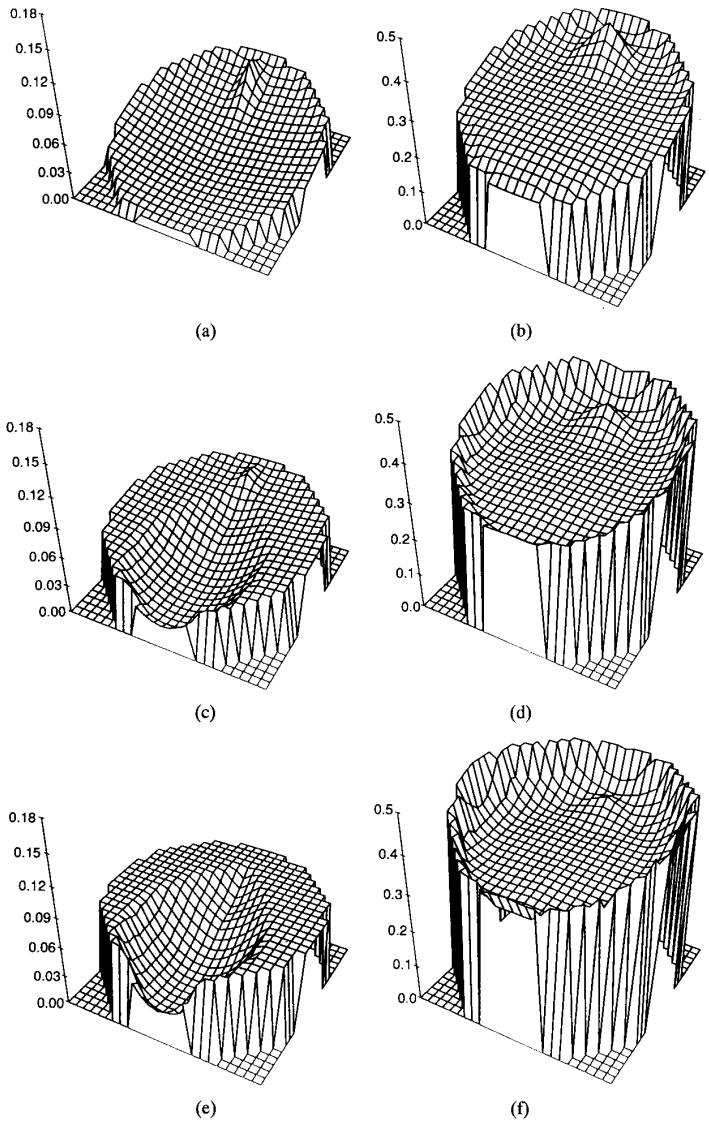

Fig. 10. BRDF's for conifer (a, c, e) in the red band and savanna (b, d, f) in the near-infrared at high cover and 55° solar zenith angle. (a)–(b): $\beta = 0.0$. (c)–(d): $\beta = 0.6$. (e)–(f): $\beta = 1.0$.

itself is controlled by several variables, of which the most important are the shape and density of plant crowns, and the contrast between the brightness of the crown and the background. The density of crowns and the brightness contrast control the magnitude of the hotspot effect, whereas its basic shape is determined by the shape of the plant crowns. That is, when the plant crown casts a shadow that is not circular, the degree to which the shadow will be revealed as the viewing position diverges from the illumination position is a function of the shape of crown and the shape of the shadow. It is important to note that since in the normal case the shadow is not circular, hotspots will, by nature, be assymetric in angle. This fact, confirmed by published suites of bidirectional reflectance factor measurements [22], [24], suggests that the common practice of simply representing the hotspot effect by a function that is dependent only on the phase angle between illumination and viewing positions [9], [13], [14], [25], [26] may be inappropriate for careful modeling of natural vegetation covers.

As to the bowl-shape of the BRDF that is also noted for discrete-canopy vegetation covers, it seems obvious from our simple mathematical modeling and Monte Carlo simulations that the basic reason for this phenomenon is that the lower parts of crowns are more likely to be hidden from both illumination and viewing at large zenith angles, whereas the upper portions are more likely to be exposed to both. Like the hotspot, the mutual-shading effect is dependent on the shape and density of plant crowns and the contrast between the brightness of the crown and the background. Although the accuracy of our model for this effect remains as yet unverified

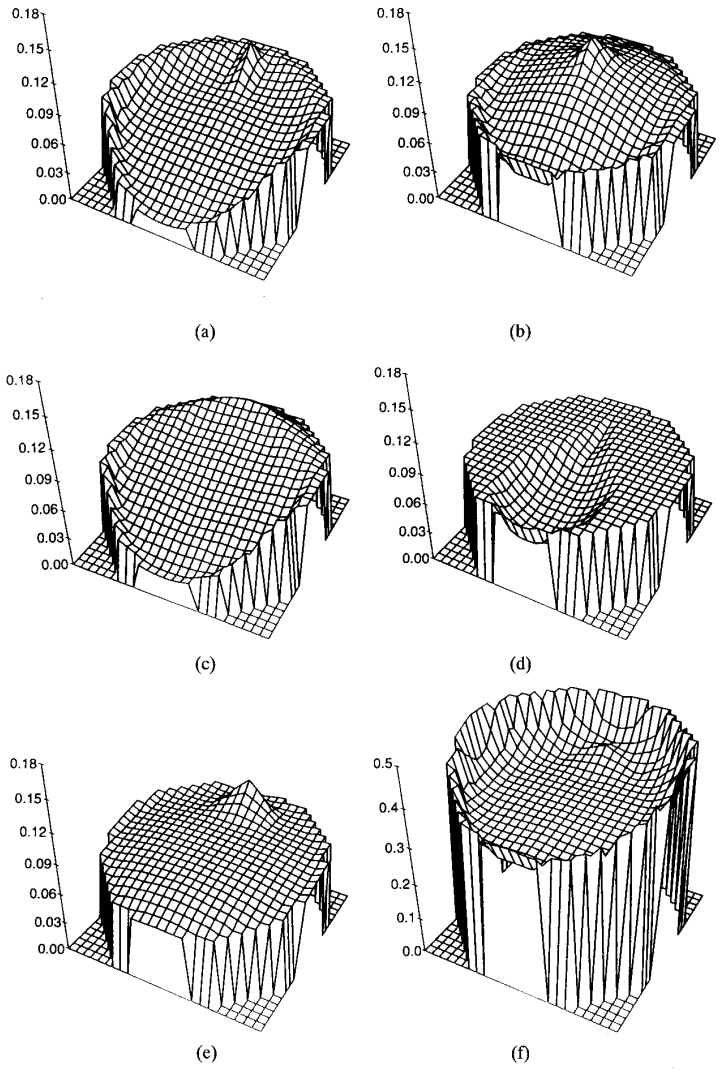

Fig. 11. BRDF's demonstrating the effect of change in illumination position, percent cover, and spectral band for strong mutual shadowing (β = 1.0). (a), (b): conifer, red band, low cover, solar zeniths 55° and 15°. (c), (d): shrub, red band, solar zenith 55°, low and high covers. (e), (f): savanna, high cover, solar zenith 55°, red and near-infrared bands.

by careful bidirectional radiance measurements, the basic agreement between modeling and simulation is encouraging.

It seems obvious that the mutual shadowing effect that produces the bowl-shaped BRDF will always occur to some extent in a vegetation cover of discrete plant crowns at any reasonable density. Thus, our random case above, in which viewing and illumination shadows are independent, is never likely to occur. In practice, the canopy will always have a top layer that dominates its BRDF at large zenith angles. At this time, we still don't know how to define such a top layer, nor how close a real canopy is to either the uniform-height or random extremes.

Another problem concerns the formulation of the parameter β, used in (24), which is still somewhat intuitive, and lacks physical meaning. Given the size, shape, height, and spacing distributions, it will not be difficult to define a depth where the probability that a crown surface element is both sunlit and viewed is, in fact, zero. But a such a depth will vary with viewing direction, which may present in problem in practical application. Nonetheless, it may still be an improvement to define a better index β from the viewpoint of gap probability.

Another limitation arises from the problem that in the uniform-height case, when coverage is high, crowns are heavily intersected. Thus, our model will become a rough-surface model. In such a case, volume scattering of crowns may be more important than surface scattering in determining the canopy BRDF, especially when the solar zenith angle is small and shadowing is minimal. A similar situation will result when the leaf area index within crowns is small or the reflectance of leaves is high and multiple scattering becomes important. In these cases, the differences between shadowed and sunlit elements may become much smaller, and thus radiative

transfer or nested geometric-optical models must be applied to determine G, C, T, and Z more precisely. Only further development of such hybrid or nested models can help us to determine where the breaking point lies between the suitability of simpler pure geometric or more complicated models, which would reflect the basic mechanisms of interaction of radiation with discontinuous canopies and yet be relatively simple for inversion.

V. Conclusion

Because many natural vegetation covers may be regarded as assemblages of plant crowns that are located on a background plane and interact with light as discrete objects, geometric optics can provide an approach to model the bidirectional reflectance distribution function of natural vegetation canopies that captures the most important features exhibited by bidirectional measurements of such canopies—notably the hotspot with its angular assymetry, produced by the uncovering of noncircular shadows as viewing and illumination positions diverge, and the bowl-shape, produced by the hiding of mutual shadows of crown on crown when view zenith angles are large. The models presented here are not exact physical descriptions of these phenomena, but are approximations that exploit the primary mechanisms relating the size, shape, and count density of plant crowns to viewing and illumination positions and crown-background reflectance contrasts. As such, they could be improved in a number of ways, but without comparison to directional reflectance measurements it is difficult to determine which improvements are most needed. Accordingly, the authors are now embarking on a program of acquisition of bidirectional reflectance measurements, both in the U.S. and the Peoples' Republic of China, that will include not only requisite radiance measurements, but also measurements of plant crowns, their locations and geometries, as well the characteristics of the leaves, branches and trunks they contain. We hope these data will guide the future development of reflectance models of many sorts and the further development of inversion procedures to extract basic information about plant canopies from remotely-sensed data.

Acknowledgment

The authors would like to thank Shunlin Liang, Xiao Yan, and Crystal Schaaf for their help in preparing the figures and graphs that accompany this paper.

References

[1] G. H. Suits, "The calculation of the directional reflectance of a vegetation canopy," *Remote Sensing Environment*, vol. 2, pp. 117–125, 1972.
[2] G. H. Suits, "The cause of azimuthal variations in directional reflectance," *Remote Sensing Environment*, vol. 2, pp. 175–182, 1972.
[3] P. Kubelka and F. Monk, "Ein beitrag zur optik der farbanstruck," *Z. Tech. Phys.*, vol. 11, pp. 593–601, 1931.
[4] W. Verhoef, "Light scattering by leaf layers with application to canopy reflectance modeling: The SAIL model," *Remote Sensing Environment*, vol. 16, pp. 125–141, 1984.
[5] E. Reyna and G. D. Bhadwar, "Inclusion of specular reflectance in vegetative canopy models," *IEEE Trans. Geosci. Remote Sensing*, vol. GE-23, pp. 731–736, 1985.
[6] D. L. B. Jupp and A. H. Strahler, "A hotspot model for leaf canopies," , *Remote Sensing Environment*, vol. 38, pp. 193–210, 1991.
[7] S. Chandrasekhar, *Radiative Transfer*. London: Oxford University Press, 1950.
[8] J. Ross, *The Radiation Regime and Architecture of Plant Stands*. The Hague: Dr W. Junk, 1981.
[9] M. M. Verstraete, B. Pinty, and R. E. Dickinson, "A physical model of the bidirectional reflectance of vegetation canopies: I. Theory," *J. Geophys. Res.*, vol. 95, pp. 11755–11765, 1990.
[10] A. S. W. Gerstl and A. C. Simmer, "Radiation physics and modeling for off-nadir satellite sensing of non-Lambertian surfaces," *Remote Sensing Environment*, vol. 20, pp. 1–29, 1986.
[11] A. C. Simmer and S. A. W. Gerstl, "Remote sensing of the angular characteristics of canopy reflectance," *IEEE Trans. Geosci. Remote Sensing*, vol. 23., pp. 648–675, 1985.
[12] R. B. Myneni, V. P. Gutchick, J. K. Shultis, G. Asrar, and E. T. Kanemasu, "Photon transport in vegetation canopies with anisotropic scattering, Part IV: Discrete-ordinates finite difference kernel technique for photon transport in slab geometry for the two-angle problem," *Agricultural and Forest Meteorol.*, vol. 42, pp. 101–120, 1988.
[13] R. B. Myneni, G. Asrar, and S. A. W. Gerstl, "Radiative transfer in three-dimensional leaf canopies," *Transport Theory and Statistical Physics*, vol. 19, pp. 205–250, 1990.
[14] A. L. Marshak, "The effect of the hot spot on the transport equation in plant canopies," *J. Quant. Spectrosc. Radiat. Transfer*, vol. 42, pp. 615–630, 1989.
[15] T. Nilson and A. Kuusk, "A reflectance model for the homogeneous plant canopy and its inversion," *Remote Sensing Environment*, vol. 27, pp. 157–167, 1989.
[16] T. Nilson and U. Peterson, "A forest canopy reflectance model and a test case," *Remote Sensing Environment*, vol. 37, pp. 131–142, 1991.
[17] X. Li and A. Strahler, "Geometric-optical modeling of a coniferous forest canopy," *IEEE Trans. Geosci. Remote Sensing*, vol. GE-23, pp. 207–221, 1985.
[18] X. Li and A. H. Strahler, "Geometric-optical bidirectional reflectance modeling of a coniferous forest canopy," *IEEE Trans. Geosci. Remote Sensing*, vol. GE-24, pp. 281–293, 1986.
[19] D. L. B. Jupp, J. Walker and L. K. Penridge, "Interpretation of vegetation structure in Landsat MSS imagery: A case study in distributed semiarid eucalypt woodlands, Part 2: Model-based analysis," *J. Environmental Management*, vol. 23, pp. 35–57, 1986.
[20] J. Serra, *Image Analysis and Mathematical Morphology*. New York: Academic Press, 1982.
[21] A. H. Strahler and D. L. B. Jupp, "Modeling bidirectional reflectance of forests and woodlands using Boolean models and geometric optics," *Remote Sensing Environment*, vol. 34, pp. 153–166, 1990.
[22] D. S. Kimes, W. W. Newcomb, R. F. Nelson, and J. B. Schutt, "Directional reflectance distributions of a hardwood and a pine forest canopy," *IEEE Trans. Geosci. Remote Sensing*, vol. GE-24, pp. 281–293, 1986.
[23] X. Li, "Geometric-optical modeling of a coniferous forest canopy," Ph.D dissertation, University of California, Santa Barbara, 1985.
[24] K. T. Kriebel, "On the variability of the reflected radiation field due to differing distributions of the irradiation," *Remote Sensing Environment*, vol. 4, pp. 257–264, 1976.
[25] A. Kuusk, "The hot spot effect of a uniform vegetative cover," *Sov. J. Remote Sensing*, vol. 3, pp. 645–658, 1985.
[26] S. A. W. Gerstl, C. Simmer, and B. J. Powers, "The canopy hot-spot as crop identifier," in *Symposium on Remote Sensing for Resources Development and Environmental Management*, Enschede, F. R. G., pp. 261–263, Aug. 1986.

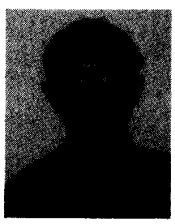

Xiaowen Li was born in Sichuan, China in 1947. He graduated from Chengdu Institute of Radio Engineering, China, in 1968. He received the M.A., M.S., and Ph.D. degrees from the University of California, Santa Barbara, in 1981 and 1985.

He has been an associate professor and Deputy Director of the Laboratory of Digital Image Processing, Institute of Remote Sensing Applications, chinese Academy of Science since 1987. He is currently Research Associate Professor at the Center for Remote Sensing, Boston University. His primary interests are in 3-D modeling and reconstruction from multiangular remotely sensed images.

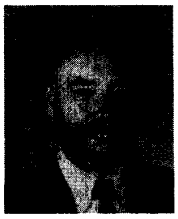

Alan H. Strahler (M'86) received the B.A. and Ph.D. degrees in geography from The Johns Hopkins University, Baltimore, MD, in 1969 and 1964, respectively.

He is currently a professor of geography and a researcher in the Center for Remote Sensing, Boston University, Boston, MA. He held prior positions at Hunter College of the City University of New York, at the University of California, Santa Barbara, and at the University of Virginia. Originally trained as a biogeographer, he has been actively involved in remote sensing research since 1978. He has been a principal investigator on numerous NASA contracts and grants. His primary research interests are in spatial modeling and spatial statistics as they apply to remote sensing, and in geometric-optical modeling of remotely sensed scenes. He is particularly interested in remote sensing of forests and the inference of vegetation canopy parameters from digital images through invertible models.